Model of Particle-Vapor Codeposition with Application to Ceramic Materials Synthesis

Robert H. Hurt and Mark D. Allendorf
Combustion Research Facility, Sandia National Laboratories, Livermore, CA 94551

The simultaneous deposition of particles and material from the vapor phase gives rise to surface deposits having characteristic structure. A mathematical model of the particle-vapor codeposition process is developed that predicts the structure and properties of these deposits as well as their growth rate over a wide range of conditions. A random sphere formulation is developed that provides the framework for a unified treatment of both subprocesses: ballistic particle deposition and porous media densification through vapor deposition. The model is applied to particle-enhanced chemical vapor deposition (PECVD) processes for the production of ceramic materials. In PECVD, particles are introduced into a CVD process, either in the form of an aerosol created in situ *by a controlled amount of gas-to-particle conversion or in the form of independently charged powder. The model identifies PECVD conditions that produce deposition rates substantially higher than those achievable by conventional CVD.*

Introduction

The inherent refractory properties of ceramics make them ideal candidates for applications requiring resistance to high temperatures and corrosive environments. The need for materials with reproducible properties, however, has led to complex, time-consuming and expensive synthesis processes. There is thus considerable incentive to develop new methods for producing these materials economically, thereby expanding their usefulness. Among the many synthesis methods explored, production of ceramics from gas-phase precursors is particularly attractive, since a wide variety of materials can be made, including oxides, nitrides, and carbides (see, for example, Ulrich 1984; Biswas et al., 1989; Spear et al., 1990; Suyama et al., 1985). In addition, the high purities required for making defect-free ceramics can also be obtained through gas-phase synthesis. Techniques are now available to form thin films or coatings (Spear et al., 1990), powders (Suyama et al., 1985; Ho et al., 1989; Alam et al., 1979), and composites (Stinton et al., 1988) from gas-phase precursors. Low deposition rates are one factor limiting the commercial application of some techniques. For example, until recently, aluminum nitride (AlN) films could be produced only at rates below 1.0 μm/min, which are inadequate for industrial production of deposits thicker than about 10 μm (Komiyama et al., 1985).

Correspondence concerning this article should be addressed to R. H. Hurt.

Recently, substantial increases in deposition rates of titanium dioxide, zirconium oxide (ZrO_2), and AlN have been reported using a technique referred to as particle precipitation-aided chemical vapor deposition (Komiyama et al., 1985, 1986, 1987; Shimogaki, 1986). The key feature of this CVD variant is the nucleation and growth of fine particles in the gas-phase during synthesis, which can occur when higher precursor concentrations are used. Coupling this aerosol formation with a substrate that is cooled relative to the gas causes fine particle deposition and CVD to occur on the substrate simultaneously. Improvements in AlN deposition rates of up to two orders of magnitude have been obtained with this technique (Komiyama et al., 1986).

The structure of deposits formed by this technique is depicted in Figure 1. It is believed (Komiyama, 1986) that reactions of gas-phase species occur on the enhanced surface area of a porous region at the interface between the growing deposit and the gas phase. Depending on the particle size and on the relative rates of particle and vapor deposition, the three-dimensional, porous interface between the fully dense deposit and the gas phase may provide a surface for heterogeneous CVD reactions several orders of magnitude greater than the smooth surface of the original substrate. There is a close relation between this process and chemical vapor infiltration (CVI) processes (Besmann et al.,1990), in which porous bodies

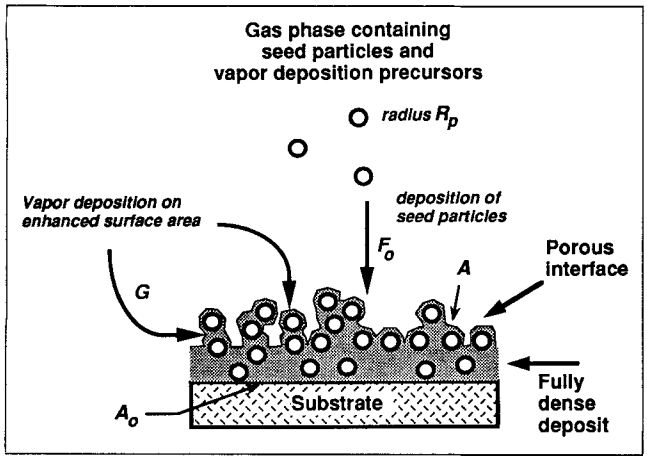

Figure 1. Particle-vapor codeposition process.

(formed, for example, from compressed powders) are densified by internal CVD growth, the difference being that in PECVD the porous body is formed gradually with CVI-type densification occurring simultaneously in a restricted region at the porous interface of the growing deposit.

In addition to formation of particles via homogeneous nucleation, particle codeposition can also be achieved by independently charging seed particles to the reactor, entrained in a gas flow (Scoville et al., 1990). This method has several advantages, including independent and accurate control over both particle loadings and gas-phase composition. In addition, one can employ particles larger than 20 μm in diameter that deposit efficiently under gravitational or inertial forces, obviating the need for a cooled substrate to drive thermophoretic deposition. (The discussion of processes, in which seed particles are independently charged to a CVD reactor, is based on an ongoing collaboration with Peter Reagan of Thermo Electron Technologies Corporation, Waltham, MA.) In this article, processes in which the rate of CVD is enhanced by the codeposition of particles, achieved either by seeding the gas phase or by a controlled amount of gas-to-particle conversion, will be referred to generically as particle-enhanced chemical vapor deposition (PECVD) processes.

A model of generic particle-vapor codeposition processes developed here is applied to PECVD processes for the synthesis of ceramic materials. The model applies directly to many deposition systems, in which the growth rate from the vapor phase is limited by the rate of surface chemical reactions. In general, CVD rates can also be limited by the rate of homogeneous gas-phase reactions or by the transport of reactive species to the substrate surface. In such cases, the present model of surface phenomena must be coupled with a model of kinetics and transport in the gas phase to predict overall rate enhancements. In effect, the gas-phase processes influence the local CVD rate that is an input into the present model. Since gas-phase processes are highly system-specific (requiring knowledge of the flow and temperature fields in the reactor and the relevant homogeneous kinetics), they are not included in this generic model of surface phenomena.

In the existing literature there have been numerous studies of particle deposition on surfaces, with application to the sedimentation of suspensions (Vold, 1960), filtration (Meakin, 1983), and coal ash deposition on boiler heat transfer surfaces (Baxter et al., 1990). The particle deposition process has been studied both experimentally and theoretically considering both diffusional trajectories (Racz et al., 1983; Meakin, 1983) and ballistic (nondiffusional) trajectories (Vold, 1960, 1963; Krug et al., 1989; Meakin, 1988). There have also been numerous studies of the vapor deposition process with application to thin-film production (Henderson et al., 1974) and to the densification of porous media by chemical vapor deposition (Besmann et al., 1990). There has not, however, to the authors' knowledge, been a theoretical treatment of the particle-vapor *codeposition* process and, as a result, the factors determining the growth rate and properties of such deposits are not well established.

In this article, a random sphere formulation is developed and used in a unified treatment of both ballistic particle deposition and densification of porous media by vapor deposition. Particle-vapor codeposition is shown by the model to produce deposits having characteristic physical features. When the rate of vapor deposition is limited by surface reactions, the deposits consist of a fully dense region and a porous region at the gas/deposit interface. This porous interfacial region contains internal surface area that is responsible for greatly enhanced growth rates relative to vapor deposition in the absence of particles. The physical properties of the deposit and the rate of growth are shown to be a function of time, deposition mechanism, and a single dimensionless parameter. The model predicts the enhanced deposition rate as well as the surface area, porosity and density profiles of the growing deposit as a function of time, given the intrinsic vapor deposition rate, the particle deposition rate, the particle size, and a specification of the particle deposition mechanism. An additional dimensionless parameter is introduced to account for mass transfer limitations in the porous interfacial region, which can prevent complete densification and result in porous, friable deposits. Scaling laws derived suggest the use of small particle size and high reactant concentration to facilitate complete deposit densification. The model results presented will serve to guide the development of PECVD processes into parameter ranges producing high-quality material at high deposition rates.

Development of the RASSPVDN Model

In this section, the random sphere model of simultaneous particle and vapor deposition (RASSPVDN) (pronounced "Rasputin") is developed. The model considers the local particle-vapor codeposition process, isolated from processes occurring prior to deposition, such as nucleation and growth of seed particles in the gas phase (which are highly system-specific). As seen in Figure 1, seed particles, which are assumed to be spheres of radius R_p, approach the growing film and deposit in the porous interface at a rate F_o (particles/cm^2·s). At the same time, vapor deposition occurs on all exposed surfaces at a uniform rate, G (μm/min). Formulated in this way, the model is applicable to vapor deposition processes that are limited by the rate of surface chemical reaction. The parameters G, R_p, and F_o completely define the deposition process, along with specification of the deposition mechanism, a topic to be discussed in a later section. The volumetric deposition rate can be defined as dV_t/dt, where V_t (cm^3/cm^2) is the total solid volume in the deposit normalized by area of the bare substrate. There are two contributions to the deposition

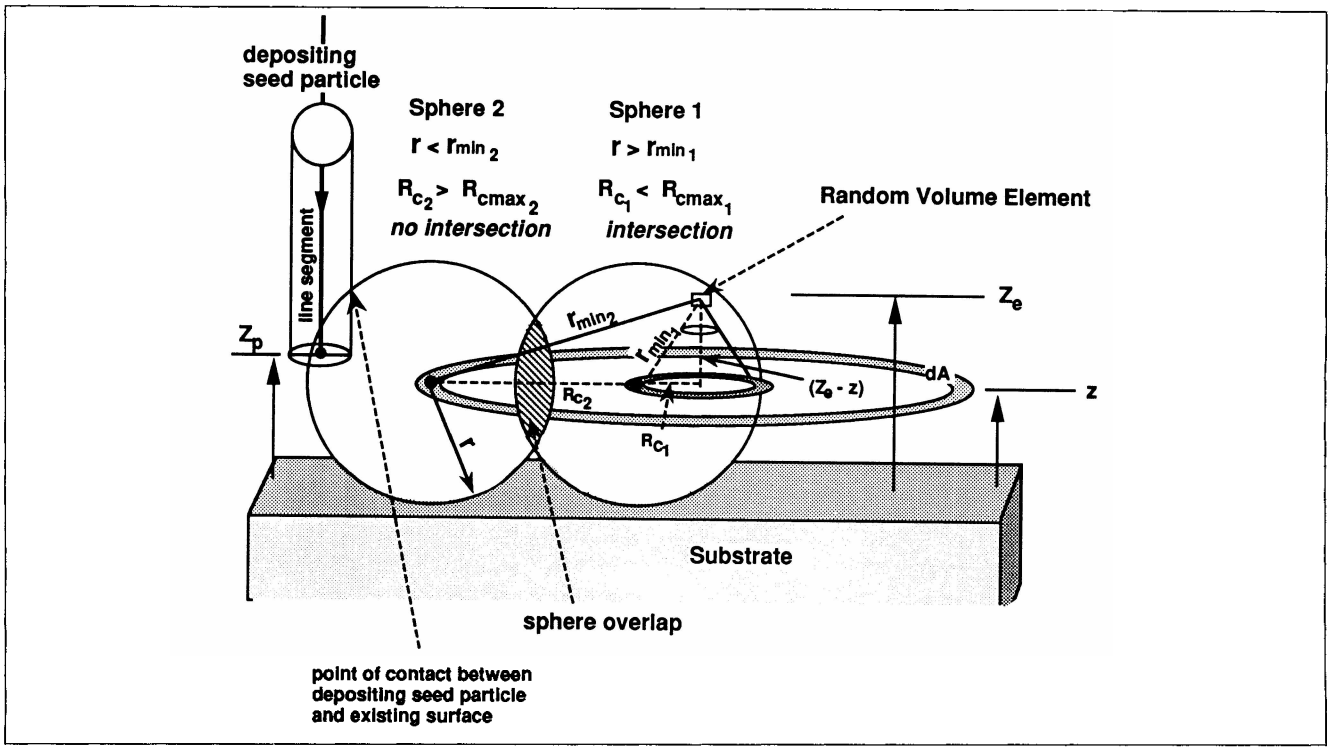

Figure 2. Random sphere formulation.

rate, the first being vapor deposition on the enhanced surface area at a rate $(A/A_o)G$, where A is the total surface area of the deposit, and the second the direct addition of solid volume through seed particle deposition $F_o(4/3)\pi R_p^3$. The total volumetric deposition rate is then given by:

$$\frac{dV_t}{dt} = (A/A_o)G + F_o\frac{4}{3}\pi R_p^3 \qquad (1)$$

The deposition rate *enhancement* is defined as the volumetric deposition rate dV_t/dt divided by G, the volumetric deposition rate for vapor deposition (CVD) in the absence of particles.

To solve Eq. 1, an accurate description of the complex geometry of the porous deposit is required to relate the amount of internal surface area to the process parameters F_o, R_p, G and the deposition time t. A mathematical approach is sought that is capable of determining the structure of deposits formed over a wide range of conditions (particle size and relative particle and vapor deposition rates). Monte Carlo techniques have been applied extensively to particle deposition processes and provide much information on the microstructure of the porous deposits (Krug et al., 1989). Unfortunately, Monte Carlo simulations are too computationally-intensive for a study of particle-vapor codeposition over the wide range of conditions of interest. Large-scale simulations and theoretical arguments indicate that the structures formed by ballistic deposition are uniform on all, but short-length, scales (Meakin, 1988). A mean field approach is, therefore, believed to be justified if it permits a unified treatment of both ballistic particle deposition and the densification of porous media by vapor deposition. In the next section, a random sphere formulation is developed, which provides the framework for such a mean field description of particle-vapor codeposition.

Random sphere formulation

Gavalas (1980) has treated the growth and coalescence of cylindrical pores during carbon gasification by a random capillary model. In a similar fashion, the growing film can be considered to consist of the original substrate surface plus the collection of all seed particles (assumed to be spheres), which have grown steadily by surface growth from the vapor phase since the time of their deposition (see Figure 1). These enlarged spheres overlap with their neighbors, producing a complex, three-dimensional porous body, whose geometry is determined completely if the sizes of all the spheres and the locations of their centers are specified. The model tracks the position, size and number density of each group of particles with identical histories and uses a statistical treatment of the collection of randomly distributed spheres to compute the deposit properties from the particle data at any instant.

It is assumed that the sphere centers are distributed randomly in space with a mean number density per unit volume $\gamma\ dr$, which is dependent upon height, z above the substrate and upon deposition time t. Since simultaneous deposition and growth lead to a deposit comprising, at any instant, spheres of many different sizes, γ will be a function of both z and r, the sphere radius. The problem is thus reduced to finding the evolution of the distribution $\gamma(r,z)$ with time and deriving expressions for the deposit properties of interest from $\gamma(r,z)$ at any instant. Properties of interest include the local solid volume fraction $V_s(z)$ (m^3/m^3), the total solid volume V_t (m^3/m^2 substrate), and the internal surface area A/A_o (m^2/m^2 substrate). Because the random distribution of the sphere centers in space allows the spheres to partially overlap as they grow, film properties such as porosity or surface area are not simple sums of the individual particle properties.

In the following paragraphs, an expression is derived for

$V_s(Z_e)$, the solid volume fraction of the deposit at a height Z_e above the substrate. To calculate $V_s(Z_e)$ or, equivalently, $1-\theta(Z_e)$, consider the random volume element at height Z_e depicted in Figure 2. The solid volume fraction in the plane at Z_e is equal to the probability P that this volume element lies within the domain of one or more of the growing spheres that constitute the deposit. If the probability is dP_s that the volume element at Z_e lies within the volume of a *single* given sphere, then by the properties of the Poisson distribution, the probability that the element lies within *none* of the spheres is

$$1-P(Z_e)=e^{(-\int dP_s)} \tag{2}$$

where the individual probabilities have been integrated over all spheres. The probability of lying within *at least one* sphere is equivalent to the solid volume fraction and is given by

$$P(Z_e)=V_s(Z_e)=1-\theta(Z_e)=1-e^{(-\int dP_s)} \tag{3}$$

To evaluate the above integral, start with a volume element dV fixed in space at height Z_e and consider the probability of intersection or overlap of this volume element with each sphere in the deposit. We first consider the probability that the volume element at Z_e is intersected by a sphere of radius r, whose center lies somewhere in the plane at distance z from the substrate surface (see Figure 2). The probability of intersection is equal to:

$$dP_{r,z,dV}(Z_e)=\gamma(r,z)dr\,dV \tag{4}$$

that is, the number density of such spheres per unit volume multiplied by the differential volume. The above equation is valid for those spheres with radii $r>r_{\min}$, where $r_{\min}$ is the distance between the volume element and the differential volume containing the sphere center. Spheres with radii $r<r_{\min}$ are not large enough to intersect the volume element:

$$dP_{r,z,dV}(Z_e)=0 \text{ for } r<r_{\min} \tag{5}$$

The technique of integrating Eq. 3 is illustrated in Figure 2. Consider a differential volume element in the shape of a ring with area in the z plane of $dA=2\pi R_c dR_c$, and a thickness dz. Equation 4 is integrated throughout the plane at z by varying the ring radius R_c from zero (corresponding to the point directly below the volume element at Z_e) to a critical value $R_{c\max}$ given by:

$$R_{c\max}=\sqrt{r^2-(Z_e-z)^2} \tag{6}$$

Any spheres of radius r encountered in rings with $R_c>R_{c\max}$ are too distant to intersect the volume element (see, for example, sphere 2 in Figure 2). The result of this integration, for a given sphere radius R, is:

$$dP_{r,z}(Z_e)=\left[\int_{R_c=0}^{\sqrt{r^2-(Z_e-z)^2}}\gamma(r,z)2\pi R_c\,dR_c\right]drdz \tag{7}$$

The solid volume fraction is now obtained by integrating over all particle radii, starting with the minimum particle radius, $r=(Z_e-z)$, for which an intersection is possible, and integrating over the entire deposit thickness yielding:

$$\ln[1-P(Z_e)]=\ln[1-V_s(Z_e)]=-\int_0^\infty\int_{|Z_e-z|}^\infty\int_{R_c=0}^{\sqrt{r^2-(Z_e-z)^2}}\gamma(r,z)2\pi R_c\,dR_c\,dr\,dz \tag{8}$$

Analytical evaluation of the innermost integral yields the final expression for the porosity or solid volume fraction at distance Z_e from the substrate:

$$V_s(Z_e)=1-\theta(Z_e)=1-e\left\{-\int_0^\infty\int_{|Z_e-z|}^\infty\gamma(r,z)\pi[r^2-(Z_e-z)^2]dr\,dz\right\} \tag{9}$$

Eq. 9 is the fundamental equation describing the geometry of the porous deposit. The total surface area of the deposit can be obtained by considering a differential amount of film growth on existing spheres:

$$A/A_o=\frac{1}{G}\frac{dV_t}{dt}\ (\text{for } F_o=0) \tag{10}$$

where V_t is the total solid volume in the deposit, obtained by integrating V_s (Eq. 9) over all z. Both A/A_o (cm^2/cm^2) and $V_t(\text{cm}^3/\text{cm}^2)$ are normalized by the area of the bare substrate A_o.

Surface growth by vapor deposition

Deposition from the gas phase also affects the distribution $\gamma(r,z)$. In the absence of diffusion limitations, there will be uniform growth on all exposed surfaces by vapor deposition (G μm/min), resulting in a steady increase in the radius of all particles present and shifting the distribution $\gamma(r,z)$ toward larger particle sizes:

$$\frac{\partial\gamma(r,z)}{\partial t}=\frac{\partial\gamma(r,z)}{\partial r}\cdot G \tag{11}$$

Simultaneously, a flat deposit grows on the original substrate surface by vapor deposition at a uniform rate, G (μm/min).

Particle deposition

The mechanism of particle deposition determines the nature of the porous interface, which in turn determines the PECVD growth rate. Two important particle deposition mechanisms will be considered.

1. *Deposition at Unity Sticking Coefficient.* Surface forces are dominant in this mechanism and particles are brought to rest at the point of first impact with any surface in the interfacial region of the growing deposit.

2. *Gravitational Settling.* In this mechanism surface forces between the particles and the deposit are negligible in comparison to gravitational or inertial forces, and seed particles may undergo multiple interactions with solid surfaces, coming to rest only at positions in the bed, at which further downward motion is impossible.

The first deposition mechanism produces loose particle packings with low particle volume fraction, while the second produces dense packings with particle volume fractions that can exceed 50% (Dullien, 1984). Which deposition mechanism is applicable in a given case is a function of the particle properties, chiefly size (Roller, 1930), density and surface roughness (Shinohara, 1984), or the presence of a liquid phase at the surface (Baxter, 1990). Any combination of large particles, high density, or smooth dry surfaces tends to promote deposition by gravitational settling.

In the model, it is assumed that approaching particles follow ballistic (nondiffusional) trajectories, an assumption that is strictly appropriate for particles that deposit by sedimentation, inertial deposition, or thermophoresis. For particles larger than about 1 μm, deposition by diffusion through a boundary layer in laminar flow is very slow (Beddow, 1980). The model also assumes that particle trajectories are orthogonal to the deposit/substrate plane, a restriction that can easily be relaxed to account for an arbitrary angle of particle approach according to system-specific flow patterns and temperature gradients. We believe that the two cases considered define the limits of PECVD behavior, when particles above about 1 μm are employed, for which convective diffusion processes, leading to gas-phase agglomeration or departure from straight deposition trajectories, are typically ineffective (Friedlander, 1977). The results presented are believed also to be qualitatively indicative of PECVD performance using very fine particles, although diffusional motion and gas-phase agglomeration may lead to some reduction in interface density and somewhat higher rate enhancements.

For each deposition mechanism, we must first consider the influence of particle deposition on the γ distribution. At a given position in the film, deposition of seed particles of radius R_p increases the particle number density at R_p and leaves the rest of the distribution unaffected.

$$\frac{\partial F(R_p,z)}{\partial z} = [1/\theta(z)]\,\frac{\partial \gamma(R_p,z)}{\partial t} \tag{12}$$

Here, $\partial F/\partial z$ is the rate at which particles leave the approaching particle stream. The appearance of the factor $1/\theta(z)$ requires some explanation. The random sphere formulation permits particles to overlap in space and thus lends itself naturally to the treatment of deposit densification by vapor deposition. However, the random sphere formulation also allows the seed particles, as they deposit, to overlap with already-deposited spheres in the interfacial region. In reality, a seed particle in the act of deposition will not overlap with existing solid in the interface, an effect which leads, for real packings, to local order and a departure from spatial randomness when considering the positions of spheres that are adjacent or nearly adjacent.

The assumptions of pseudo-steady state and a monodisperse-size distribution of seed particles result in an ordinary differential equation for $F(R_p,z)$. By the random sphere formulation, the addition of a new seed particle to the plane at z results in a volume addition to the deposit of $(4/3)\pi R_p^3\theta(z)$ and an overlap volume of $(4/3)\pi R_p^3[1-\theta(z)]$, where $\theta(z)$ is the local deposit porosity. The unwanted overlap can be compensated for, in an approximate manner, by increasing the local number density of depositing seed spheres $\gamma(r,z)$ by the multiplicative factor $[1/\theta(z)]$ to give the correct rate of volume addition, $(4/3)\pi R_p^3$. The correction factor is typically small, because the seed particles tend to deposit in partially filled layers with low solid volume fraction (the deposition process slows rapidly as the solid volume fraction approaches a value between 0.1 and 0.5, depending on deposition mechanism).

As the upper layers of the deposit are highly porous, the deposit-gas interface is not sharp, and the depth of penetration of the depositing seed particles is a critical parameter. For a flux of approaching seed particles F_o of radius R_p we seek a continuous function $F(R_p,z)$ that describes the rate at which the flux is attenuated from F_o to zero with penetration depth, as an increasing number of the particles come to rest against solid surfaces in the interface region. The function F will depend on the mechanism of deposition and on the local deposit properties. In the following section, the random sphere approach will be used to describe deposition at unity sticking coefficient, yielding a rigorous solution for $F(z)$ as a function of particle size and $\gamma(r,z)$. In the subsequent section, a solution for $F(z)$ will be proposed to represent deposition by gravitational settling.

Ballistic Particle Deposition at Unity Sticking Coefficient. The probability that a seed particle penetrates to at least height Z_p above the substrate surface can be obtained within the random sphere formulation as follows. Let a vertical line segment extending from above the interface to height Z_p represent the trajectory of the center of an approaching seed particle (see Figure 2). The periphery of the seed particle sweeps out a cylinder of radius R_p, which must not intersect any solid surface in the deposit for the seed particle to successfully traverse the path to Z_p. We seek the probability $P_t(Z_p)$ so that this cylinder does not intersect any surface in the deposit. In practice, it is mathematically equivalent and computationally convenient to enlarge each of the existing spheres in the deposit by R_p and compute the probability that the line segment itself (instead of the cylinder) intersects any of the enlarged spheres. If the probability is $P_t(Z_p)$, that a sphere successfully reaches Z_p without encountering a solid surface, the flux profile is given by $P_t(Z_p) = F(R_p,Z_p)/F_o$.

The probability $P_t(Z_p)$ can be computed in two parts. Spheres whose centers lie at $z<Z_p$ will necessarily intersect the point Z_p if they intersect the line segment at any point. The probability of intersection by these spheres can, therefore, be obtained by an expression similar to that for the porosity at Z_p, integrating in z, but only from 0 to Z_p:

$$P_l(Z_p) = e\left[-\int_{z=0}^{z=Z_p}\int_{r=|Z_p-z|}^{r=\infty} \gamma(r,z)\pi \times \{r^2-(Z_p-z)^2\}\,dr\,dz \right] \tag{13}$$

where P_l indicates the probability contribution of the "lower" spheres (those having centers below Z_p). Above Z_p, all spheres intersecting the line segment will necessarily intersect the segment in the z-plane in which their centers lie. The probability of intersection can, therefore, be obtained by the integral:

$$P_h(Z_p) = e\left[-\int_{z_p}^{\infty}\int_{R_s}^{\infty} \gamma(r,z)\pi r^2 dr\,dz \right] \tag{14}$$

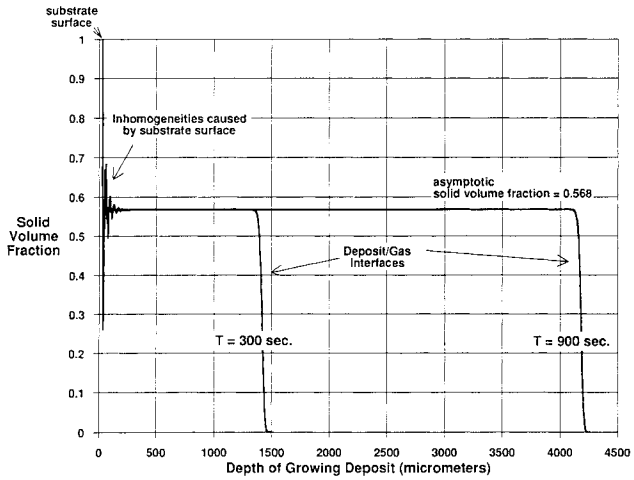

Figure 3. Profiles of solid volume fraction in a simulated random packing of spheres.

Deposition of 50-μm-diameter particles on a bare substrate by gravitational settling according to Eq. 15 with $B=0.5$.

The total probability of no intersection overall is $P_t(Z_p)=(P_l \cdot P_h)$, and the probability of at least one intersection is $1-P_t(Z_p)$. Equations 13 and 14 together can be used to evaluate the deposition profile $F(z)/F_o$ for a deposit with known $\gamma(r,z)$. Spheres packed according to this mechanism (in the absence of vapor deposition) yield beds of approximately 10% solid volume fraction. A volume fraction of 10% for orthogonal ballistic deposition at unity sticking coefficient agrees well with the value of 12.5% found by Vold (1960) using Monte Carlo simulation. A solid volume fraction of 10% (void fraction 90%) is a typical experimentally observed value for packings of fine particles ($d< \sim 1$ μm), such as fine ceramic powders, for which surface forces are strong compared to gravitational forces.

Particle Deposition by Gravitational Settling. This mechanism is operative when surface forces are negligible in comparison to gravitational or inertial forces. Here, seed particles may undergo multiple interactions with solid surfaces in the deposit, rolling downward and laterally, and coming to a final rest only at a position in the bed that prevents further downward motion. Such a resting place for a perfect sphere requires three or more points of contact with the existing spheres constituting the deposit. A detailed description of this random process involving multiple interactions among randomly oriented spheres is beyond the scope of this work. In this section, an empirical relation that mimics the random packing of large spheres by sedimentation is proposed.

Consider a regular array of packed spheres with the lattice sites in its outer layer partially occupied. Potential deposition sites in this array must offer three points of contact to an incoming sphere and must therefore consist of at least three adjacent occupied sites. By analogy to surface chemical kinetics, the fraction of such sites (or the probability of encountering such a site) may be expected to be related to the third power of the fraction of occupied sites. Motivated by this argument, we postulate that the probability that a sphere comes to rest at a depth Z_p can be related to the cube of the solid volume fraction in the underlying layer of particles:

$$\frac{dF}{dz}=F\,B[1-\theta(Z_p-R_p)]^3 \tag{15}$$

where B is an empirical constant to be determined.

To illustrate the properties of Eq. 15, the deposition of 50-μm-diameter particles on a bare substrate was simulated numerically (using $B=0.5$ for this example), and the axial porosity profile of the generated particle bed is plotted in Figure 3. The profiles show a steady-state solid volume fraction of 0.57 in the bulk of the deposit with a well defined interfacial region of 1–2 particle diameters. A value of 0.5 for B is seen to yield solid volume fractions that are typical of some random packings of spheres in the absence of surface forces (Dullien, 1984). Near the substrate surface, fluctuations around the steady-state packing density are observed, which diminish in amplitude with increasing distance from the substrate. This is a consequence of the discontinuity at the substrate surface, which promotes ordered layering near the substrate. Only after 3–4 particle diameters does this tendency toward ordered layering give way to random packing and homogeneous deposit properties. Such cyclic variations in local solid or void fraction near external surfaces have been observed experimentally (Benenati et al., 1962; Roblee et al., 1958), typically extending 3 to 4 particle diameters into the packing, in agreement with the results in Figure 3.

The mean solid volume fraction (or void fraction) obtained for a random packing of spheres depends to some extent on its method of production. The following categories of random packings and their respective void fractions have been observed (Dullien, 1984): close random packing (following vibration) with $\theta=0.359$ to 0.375, poured random packing with $\theta=0.375$ to 0.391, and loose random packing (rolling deposition of individual particles) with $\theta=0.4$ to 0.41. Solid volume fractions of 0.65 (35% void fraction) have been reported (Leva, 1959) for beds of monodisperse, randomly packed spheres in the absence of wall effects.

A value of the empirical constant B must be found that mimics these results for the random packing of large spheres. In Figure 4, the steady-state solid volume fraction is plotted vs. the empirical constant B in dimensionless form, BR_p. A

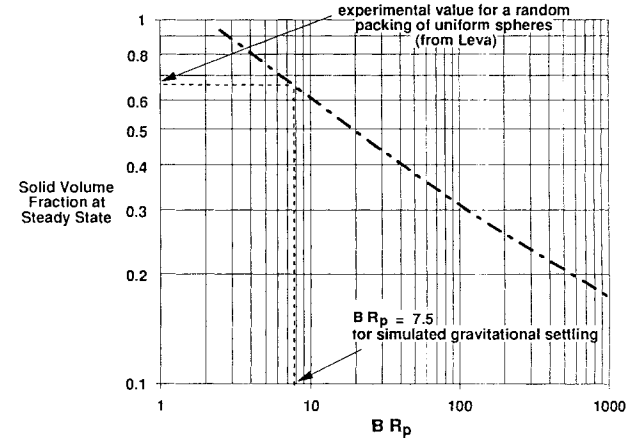

Figure 4. Asymptotic solid volume fraction for simulated deposition according to Eq. 15 for various values of BR_p.

Dotted line indicates value of BR_p required to match the experimentally packing fraction observed by Leva (1959).

value of 35% voidage or 65% solid volume fraction was taken as an upper limit on packing densities commonly observed and the corresponding *BRp* value of 7.5 was used to generate all subsequent model results for the case of gravitational settling. With this choice, the two deposition mechanisms considered span the range of common packing densities (10–65%) and provide useful limiting cases, between which most practical systems will fall.

Nondimensionalization and derivation of analytical limits

In this section, the model equations will be nondimensionalized, reducing the number of independent parameters to one and providing useful scaling laws. Adopting the following definitions: $\rho \equiv r/R_p$, $\zeta \equiv z/R_p$, $\tau \equiv tG/R_p$, $\Psi \equiv R_p{}^4\gamma$, $\alpha \equiv AR_p$, $\Omega \equiv V_t/R_p$, Eqs. 1, 9–12 and 15 become:

$$\frac{d\Omega}{d\tau} = (A/A_o) + \frac{4}{3}\pi\left[\frac{F_o R_p^3}{G}\right] \tag{16}$$

$$V_s(\zeta_e) = 1 - \theta(\zeta_e) = 1 - e\left[-\int_0^{\infty}\int_{|\zeta_e-\zeta|}^{\infty} \Psi(\rho,\zeta)\pi\{\rho^2 - (\zeta_e-\zeta)^2\}\,d\rho\,d\zeta\right] \tag{17}$$

$$A/A_o = \frac{d\Omega}{d\tau} \text{ for } (F/F_o)(1,\zeta) = 0 \tag{18}$$

$$\frac{\partial\Psi(\rho,\zeta)}{\partial\tau} = \frac{\partial\Psi(\rho,\zeta)}{\partial\rho} \tag{19}$$

$$\left[\frac{F_o R_p^3}{G}\right]\frac{d(F/F_o)(1,\zeta)}{d\zeta} = (1/\theta(\zeta))\,\frac{\partial\gamma(1,\zeta)}{\partial\tau} \tag{20}$$

Clearly, the evolution of deposit properties in dimensionless time τ is a function only of the one parameter $F_oR_p{}^3/G$, the dimensionless rate of particle deposition. This realization leads immediately to important scaling laws, which will be discussed later.

It is possible to derive analytical limits for the steady-state area and rate enhancements that are valid at high particle deposition rates (i.e., high $F_oR_p{}^3/G$). At high $F_oR_p{}^3/G$, particle deposition is complete at a given location before significant densification occurred. The deposition of particles is then unaffected by the vapor deposition within the interfacial region, leaving, in the wake of the moving deposit surface, a region of packed spheres to be densified. This region has a solid volume fraction that is equivalent to that in a bed of particles deposited in the absence of vapor deposition: 0.65 for gravitational settling and 0.1 for deposition at unity sticking coefficient. In this case, the steady-state growth rate is simply:

$$\frac{1}{G}\frac{dV_t}{dt} = \frac{F_o\frac{4}{3}\pi R_p^3}{V_{so}G} \tag{21}$$

where V_{so} is the solid volume fraction in a bed of spheres deposited by the appropriate mechanism. Results of the numerical simulations will reveal the value of $F_oR_p{}^3/G$, above which the complete solution approaches this analytical limit.

Surface reaction and diffusion within the porous interfacial region

At the high particle deposition rates necessary to achieve rapid growth, diffusional limitations may arise in the porous interfacial region, which lead to a progressive depletion of reactant from the top to the bottom of the interface. The resulting reduction in the CVD rate within the interface can prevent complete densification of the deposit, yielding a friable porous coating with inferior properties. To derive scaling laws that identify conditions that avoid mass transfer limitations within the interfacial region, assume that the rate of surface growth by vapor deposition (for example, CVD) is proportional to surface area and to C^n where n is the reaction order and C is the concentration of a gas-phase species that may be the starting material or a gas-phase intermediate (such as a decomposition product). The interplay between surface reaction and diffusion within the interface can be described as:

$$D_{\text{eff}}\frac{\partial^2 C}{\partial z^2} = k_s C^n a_v(z) \tag{22}$$

Here, k_s is an intrinsic rate constant for the CVD reactions, and a_v is the local area per unit volume. The effective diffusion coefficient in the porous medium D_{eff} is given by $D\theta/\tau_f$, where τ_f is an empirical tortuosity factor which ranges from 3 to 7 for many porous catalyst supports (Satterfield, 1981). The intrinsic rate constant that appears in Eq. 22 can be defined in terms of the local film growth rate $g(z)$ by:

$$g(z) = k_s C^n\left(\frac{v_m}{\chi}\right) \tag{23}$$

where χ is the stoichiometric factor (mole reactant/mole product) and v_m the molar volume of the solid product. With the following definitions: $C' = C/C_o$; $\zeta = z/R_p$; $g' = g/G$; $a_v' = a_vR_p$, the dimensionless equation describing reaction and diffusion becomes:

$$\frac{\partial^2 C'}{\partial\zeta^2} = \left[\frac{R_pG\chi}{C_oD_{\text{eff}}v_m}\right]C'^n a_V'(\zeta) \tag{24}$$

where C_o is the bulk concentration of species R. Equation 23 introduces a second dimensionless group $[R_pG\chi/C_oD_{\text{eff}}v_m]$ required to describe PECVD in the presence of diffusion limitations in the interface. The complete set of equations for diffusion-limited PECVD are obtained by replacing G with $g(z)$ in Eq. 11, imposing the condition $g(z) = G$ on Eq. 10 and rewriting Eq. 1 as:

$$\frac{dV_t}{dt} = \left(\frac{dV_t}{dt}\right)_{F_o=0} + \frac{F_o\frac{4}{3}\pi R_p^3}{G} \tag{25}$$

Two important scaling laws are obtained readily by considering the simplified case of a first-order reaction and an interface with a homogeneous pore structure. The solution to the reaction/diffusion in a uniform slab of thickness H is:

$$\eta = \tanh\phi_L/\phi_L;\ \phi_L = H\sqrt{k_s a_v/D_{\text{eff}}} \tag{26}$$

The effectiveness factor η is the observed reaction rate divided by the intrinsic rate at the bulk reactant concentration, C_{ro}, and ϕ_L is the Thiele modulus. For a slab with a homogeneous pore structure: $a_v = A/(A_o H)$ and substituting Eq. 23 for k_s yields for the Thiele modulus:

$$\phi_L = \left[\frac{(A/A_o)G\chi H' R_p}{C_o v_m (D\theta/\tau)}\right]^{\frac{1}{2}} \tag{27}$$

Noting that an increase in Thiele modulus corresponds to an increase in the severity of diffusion limitations, Eq. 27 can be used to examine the influence of reactant concentration, particle size and pressure on the extent of diffusion limitations and thus the ability to produce fully dense deposits (see the Discussion section).

Description of the RASSPVDN program

A numerical procedure has been developed to solve the random sphere model for deposition in the kinetically controlled regime. The RASSPVDN FORTRAN code performs the following sequence of computations: during a given time step, the deposition profile within the interface $F(z)$ is solved for a given mechanism by the fourth-order Runga-Kutta technique, and the values of $F(z)$ are then used to calculate the new particle density distribution $\gamma(r,z)$. The total solid volume fraction V_t is then calculated for the deposit by integrating V_s from the random sphere Eq. 9 over all z. An incremental amount of growth by vapor deposition is then carried out both on the substrate and on the deposited seed particles causing a shift in the $\gamma(r,z)$ distribution. This completes the time step, and deposit properties are now evaluated according to Eqs. 9 and 10. The surface area and rate enhancement factor are computed knowing the solid volume fractions before and after the growth step by vapor deposition according to Eq. 10, after which a new time step is initiated.

For seed particles of 25-μm radii and a growth rate by vapor deposition of 1 μm/min, grid spacings that produced accurate results in reasonable times were $\Delta r = 1$ μm and $\Delta z = 5$ μm. The program chooses Δt automatically to produce an amount Δr of growth by vapor deposition in one time step. A fivefold reduction in both the r and z grid spacings slowed the computations considerably, but had no significant effect on the growth rates or deposit properties.

Results

Model results are presented in Figures 5–9, whereby emphasis is placed on elucidating the factors determining the growth rate enhancement in PECVD processes. There are two components to the deposition rate enhancement: 1) the enhancement of the surface are for vapor deposition and 2) the direct deposition of solid contained in the seed particles. In Figure 5, the time evolution of the surface area enhancement A/A_o is plotted for various values of the parameter $F_o R_p^3/G$. At time $=0$, the substrate surface is bare and A/A_o is unity for all values of $F_o R_p^3/G$. As particles deposit, the porous interface develops and A/A_o rises, eventually reaching an asymptotic value corresponding to the establishment of a self-

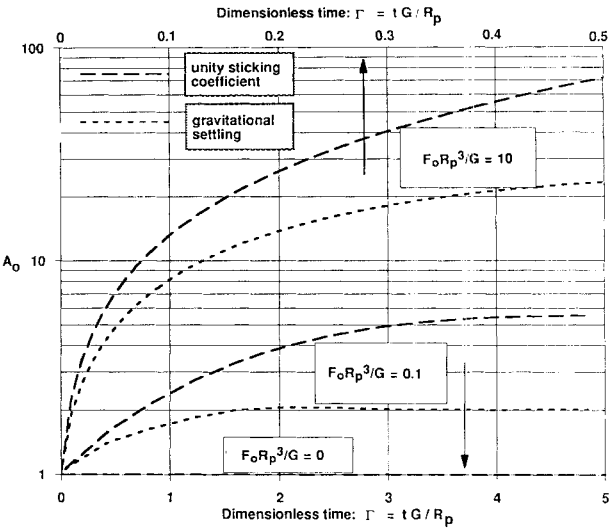

Figure 5. Evolution of deposit surface area with dimensionless deposition time.

preserving interface. A steady-state condition has been achieved with respect to the interface structure and the film growth rate. As an illustration of the time required to develop the self-preserving interface, consider the specific conditions: $F_o = 10.67$ $\text{cm}^{-2}\cdot\text{s}^{-1}$, $G = 1$ μm/min, and $R_p = 25$ μm ($F_o R_p^3/G = 0.1$). Under these conditions, 37 minutes are required to reach 50% of the steady-state area enhancement.

Figure 6 shows the magnitude of the area enhancement at steady state for a wide range of $F_o R_p^3/G$. The solid lines are results of the numerical model and the dashed lines are the analytically derived limits (Eq. 21) valid at high $F_o R_p^3/G$. Deposition with unity sticking coefficient gives higher surface area enhancements by factors of up to 6.

The contribution of the seed particle volume to the total rate enhancement is plotted in Figure 6 for comparison to the con-

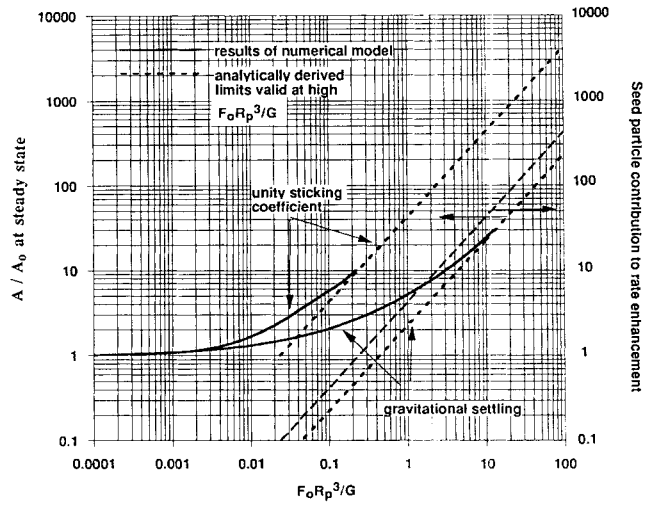

Figure 6. Total deposit surface area at steady state as a function of $F_o R_p^3/G$.

Solid lines, full numerical solutions; fine dashed lines, analytical limits valid at high $F_o R_p^3/G$, course dashed line, seed particle contribution to growth rate enhancement for comparison to surface area contribution.

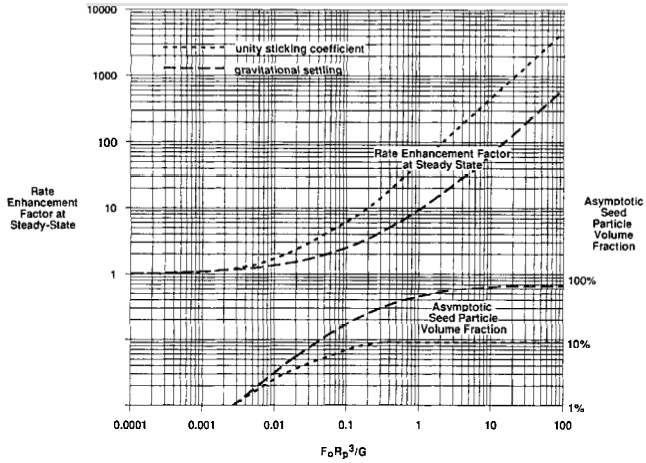

Figure 7. PECVD rate enhancement factor and seed particle volume fraction at steady state vs. $F_oR_p^3/G$.

Dashed lines, deposition by gravitational settling; dotted lines, deposition with unity sticking coefficient.

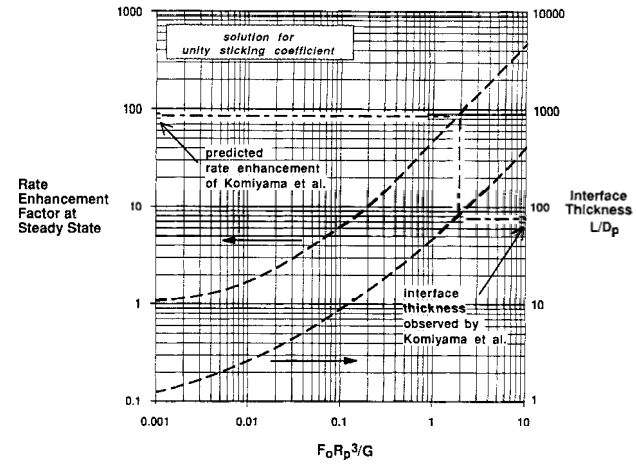

Figure 9. Interface thickness and rate enhancement factor at steady state vs. $F_oR_p^3/G$.

Dashed lines, model predictions for deposition with unity sticking coefficient; dashed/dotted line, comparison with the experimental observations of Komiyama (1985).

tribution from enhanced surface area. For unity sticking coefficient, the contribution of seed particle volume is always less than 10% of the total rate enhancement (the remainder being enhanced area for CVD). For gravitational settling, the particle contribution is small at low $F_oR_p^3/G$, but rises to 65% of the total rate enhancement at high $F_oR_p^3/G$.

The total rate enhancement, consisting of the area enhancement plus the seed particle contribution also rises with time to an asymptotic, steady-state value. The steady-state rate enhancement factor is presented in Figure 7 along with the seed particle volume fraction in the steady-state deposit. The simulations show that substantial increases in deposition rate are possible when particles are codeposited with the matrix during CVD. Rate enhancements remain less than a factor of 2 up to a dimensionless particle deposition rate ($F_oR_p^3/G$) of 0.01, thereafter increasing rapidly with increasing $F_oR_p^3/G$.

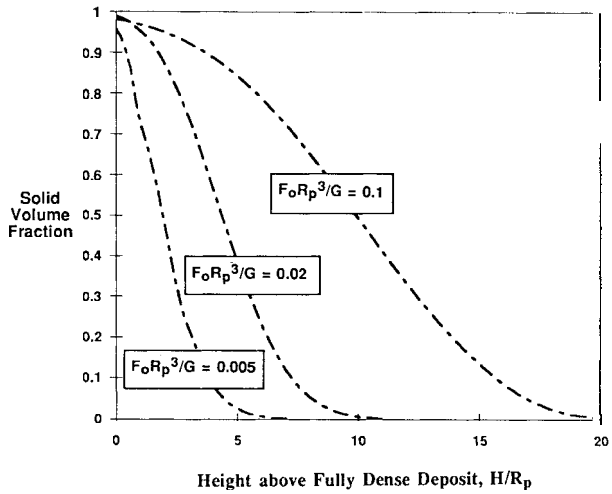

Figure 8. Self-preserving profiles of solid volume fraction at the interface of the growing deposit for various $F_oR_p^3/G$.

Particle deposition with unity sticking coefficient.

The seed particle volume fraction increases with $F_oR_p^3/G$ to a steady-state value, which depends on the deposition mechanism. The limiting seed particle volume fraction is equivalent to the solid volume fraction in a bed of particles, deposited in the absence of vapor deposition: 0.65 for gravitational settling, approximately 0.1 for deposition at unity sticking coefficient. This equivalence reflects the fact that, at high particle deposition rates, particle deposition is complete at a given location before CVD densification has proceeded there to any significant extent. The deposition of particles is then unaffected by the presence of CVD in the interface, leaving, in the wake of the moving deposit surface, a region of packed spheres to be densified. This asymptote indicates that high PECVD rates are theoretically possible (with rate enhancements over 2 orders of magnitude), while maintaining relatively low seed particle volume fractions (approximately 10% for deposition at unity sticking coefficient).

Steady-state, self-preserving profiles of the solid volume fraction at the interface are plotted in Figure 8 for deposition at unity sticking coefficient at various values of $F_oR_p^3/G$. Increasing $F_oR_p^3/G$ increases the width of the interfacial region. Defining the interface as the portion of the deposit having local solid volume fractions (or porosities) between 5 and 95%, the interface is approximately two particle diameters thick at $F_oR_p^3/G = 0.005$ and 8.5 particle diameters thick at $F_oR_p^3/G = 0.1$.

The model results in Figure 9 illustrate the direct relationship between the rate enhancement and the width of the porous interfacial region over a wide range of $F_oR_p^3/G$.

Discussion

Deposit growth rates

Results of the model illustrate that particle-vapor codeposition produces deposits having characteristic physical features. When the rate of vapor deposition is limited by surface reactions, the deposits consist of a fully dense region and a porous region at the gas/deposit interface. This porous interfacial region contains internal surface area which is responsible for

enhanced growth rates relative to vapor deposition in the absence of particles. The model predicts the existence of a unique, direct relationship between the growth rate enhancement in the kinetically controlled regime and the single dimensionless parameter $F_oR_p^3/G$. The extent of the rate enhancement at a given value of $F_oR_p^3/G$ is a function of the deposition mechanism, which in turn depends on the surface properties of the materials involved. This difference can be understood by considering the behavior of particles depositing by the two mechanisms in the absence of CVD. Gravitational settling in the absence of CVD produces sphere packings with high solid volume fractions (up to 0.65). This same mechanism produces, during particle-vapor codeposition, relatively dense interfaces, which grow in height slowly. In contrast, deposition at unity sticking coefficient produces lower density packings ($V_s \sim 0.1$) and, in codeposition, low-density interfaces, which grow rapidly. Under most conditions, the enhanced surface are is responsible primarily for the growth rate enhancement, the contribution of the seed particles being much smaller.

The two mechanisms considered (deposition at unity sticking coefficient and deposition by gravitational settling) serve as practical limits for very small and very large particles, respectively, and provide a useful range of predicted values for material systems with unknown particle deposition behavior. The precise particle size range that corresponds to a given mechanism depends on material properties, including density, surface roughness, and the presence of a liquid third phase. As a general rule, however, gravitational settling will often be the dominant mechanism for particles larger than ~ 30 μm in diameter, and the unity sticking coefficient formulation will be relevant for particles smaller than ~ 1 μm.

Seed particle volume fraction

Seed particle volume fractions are predicted to increase with increasing rate enhancement up to an asymptotic value that depends on the deposition mechanism. It is, therefore, theoretically possible to achieve high rate enhancements while maintaining relatively low seed particle fractions in the final deposit. The use of very fine particles, in particular, those which deposit with sticking coefficients near unity, should limit the volume fraction of seed material required to approximately 10%.

Effect of seed particle size

The RASSPVDN model provides a number of valuable predictions regarding the role of seed particle size. First, the model results indicate that the steady-state rate enhancement depends only on the dimensionless parameter $F_oR_p^3/G$ or, for a given vapor deposition (CVD) rate, only on the rate of addition of particle volume, $F_o(4/3)\pi R_p^3$. The steady-state rate enhancement is, therefore, *independent* of particle size at constant mass or volumetric particle feed rate. In view of the higher specific surface area of smaller particles, this result is somewhat counterintuitive. Note that the seed particles of interest to PECVD range in size from submicron aerosols to coarse powders and cover a correspondingly wide range of specific surface area. This scaling behavior is valid when the deposition mechanism remains the same. Since particle size influences the deposition mechanism, small to moderate increases in steady-state rate enhancement may indeed occur in practice as one progresses from powders to particles in the aerosol size range (see Figure 7).

The second effect of particle size regards the surface properties of the deposit. The model predicts that high rate enhancements will be accompanied by porous interfacial zones of significant thickness, which could lead to rough and friable surfaces of PECVD deposits. Improved surface properties may be obtained by densifying the interface by CVD (in the absence of particles) at the end of the coating process. The time required for "post-densification" can, according to the model, be a significant fraction of the total production time. Since the densification time scales as $t \sim G/R_p$, the time required for post-densification of the porous interface (using CVD in the absence of particles) is inversely proportional to particle size. An interface composed of small particles densifies quickly due to the small characteristic size of the voids to be filled by CVD. The use of finer particles does, therefore, bring about a significant "rate enhancement," in the form of a reduction in the time required for postdensification.

An important advantage to the use of fine particles is the potential for coating three-dimensional objects. For larger particles, the relative importance of gravitational forces makes particle impaction and sticking on vertical or downward facing surfaces difficult. In practice, the use of fine aerosols will, however, require substrate cooling and careful temperature control to promote deposition by thermophoresis while maintaining surface temperatures high enough for rapid CVD. Finally, the use of fine particles will promote mass transfer in the porous interface and thus facilitate complete densification.

Role of mass transfer limitations

In the kinetically controlled regime, arbitrarily large rate enhancements are possible by operating at very high dimensionless particle deposition rates $F_oR_p^3/G$. In practice, the finite rate of transport or of homogeneous gas-phase reactions may limit the rate at which *fully dense material* can be deposited. Kinetics and transport within the gas phase can be influenced by adjusting reactor operating conditions (flow rates and temperature fields) in an attempt to accommodate the high PECVD deposition rates. These gas-phase processes, which are highly system-specific, must be treated on a case-by-case basis and the results coupled with the present generic model of surface phenomena.

Transport limitations may also arise within the porous interfacial zone in the deposit itself. Diffusion limitations within the interface will reduce the concentration of the reactive species and thus the densification rate at points far from the deposit surface, resulting in porous, friable, low-quality coatings. The scaling laws derived indicate that the use of high reactant concentration and/or small particle size will promote efficient mass transfer through the interface and the production of fully dense material at high growth rates.

Equation 27 can be used to establish several scaling laws that elucidate the influence of reactant concentration, particle size, and pressure on the extent of diffusion limitations and thus the ability to produce fully dense deposits. The scaling laws indicate the propensity for mass transfer limitations at constant CVD rate, G, and constant PECVD growth rate, dV_t/dt. The constancy of G and dV_t/dt implies the constancy of $F_oR_p^3/G$, A/A_o, and the values of all other dimensionless

parameters. If particle size is now varied, only D and R_p in Eq. 27 may vary, resulting in: $\phi_L = (R_p/D)^{1/2}$. For large R_p, the characteristic pore size in the interface will be large and molecular diffusion will dominate: $D \sim R_p^0$ and thus $\phi_L \sim R_p^{1/2}$. Decreasing R_p will, therefore, be effective at alleviating diffusion limitations and promoting complete densification. As R_p is decreased progressively, a point may be reached where molecular diffusion gives way to Knudsen diffusion in the fine pores. In this regime, $D \sim R_p$ and $\phi_L \sim R_p^0$ and no advantage may be derived from further reduction in particle size.

The influence of total pressure can be examined using Eq. 27 in a similar fashion. At constant mole fraction of reactant pressure scaling law from Eq. 27 is $\phi_L = (1/C_{Ro}D)^{1/2}$. In the molecular diffusion regime (large R_p) $D \sim P^{-1}$, $C_{Ro} \sim P^1$, and $\phi_L \sim P^0$, whereas in the Knudsen regime (small R_p) $D \sim P^0$ and $\phi_L \sim P^{-1/2}$. An increase in total pressure may, therefore, promote complete densification for PECVD if fine particles are used, but will have no effect when using larger particles. The precise particle sizes at which these transitions occur are system-dependent.

Finally, increasing the mole fraction of reactant (which implies a decrease in temperature to achieve constant G) will also be effective at promoting mass transfer through the interface. Complete deposit densification may also be hindered by the presence of trapped or isolated porosity in the interface region. Using percolation theory, Elam et al. (1984) have computed a threshold value of 0.968 for the solid volume fraction in a bed of randomly oriented, overlapping spheres, at which point the remaining porosity (about 3%) no longer forms an infinite network. For a porous region of finite size it can, therefore, be expected that some residual porosity (< about 3%) will remain as isolated pores even for the case of growth in the kinetically controlled regime. Annealing processes would be required to eliminate this final residual porosity that has lost contact with the gas phase.

Comparison to literature

The existing experimental database in the literature for PECVD processes is quite limited. Previous studies *do* report high deposition rates, but the experiments conducted were not designed to provide an unambiguous measurement of the rate enhancement nor to control precisely particle size or particle deposition rates. Nevertheless, a qualitative comparison with some published data (Komiyama et al., 1985) will be attempted, where AIN films were grown at high deposition rates by co-deposition of AIN particles. Submicron AIN particles formed *in situ* by homogeneous nucleation were deposited on a cooled substrate by thermophoresis in the presence of CVD. Film growth rates were quoted to be several orders of magnitude greater than those reported previously using conventional CVD. An SEM (scanning electron microscope) micrograph of a deposit cross-section shows the presence of a porous interface between the gas phase and the dense material, which is composed of particles of 0.1 μm in diameter or less with a thickness of 5 to 10 μm (50 to 100 particle diameters).

In Figure 9, the steady-state rate enhancement factors and interface thicknesses (for deposition with unity sticking coefficient) are presented on a common plot. From the fine dashed line, it can be seen that an average interface thickness of 75 particle diameters corresponds to a rate enhancement of 85, roughly two orders of magnitude, in agreement with the claims of Komiyama et al. Under other conditions, deposits are reported (Komiyama et al., 1985) with less extensive interfaces, but information available from these runs is insufficient for a comparison with model predictions. While recognizing the obvious limitations of comparisons of this nature, it is nevertheless important to note that porous structures such as those postulated have been observed and associated with rate enhancements of the same approximate magnitude as those predicted by the model.

Conclusions

Several important processes involve the deposition of particles on surfaces with simultaneous deposition of material from the vapor phase. This particle-vapor codeposition is shown here to produce deposits having characteristic physical features. When the rate of vapor deposition is limited by surface reactions, the deposits consist of a fully dense region and a porous region at the gas/deposit interface. This porous interfacial region contains internal surface area, which is responsible for enhanced growth rates relative to vapor deposition in the absence of particles. The physical properties of the deposit and the rate of growth are shown to be a function of time, deposition mechanism, and the single dimensionless parameter, $F_o R_p^3/G$. An additional dimensionless parameter is introduced to account for mass transfer limitations in the porous interfacial region, which can prevent complete densification and result in porous, friable deposits. The results of the model are applied to particle-enhanced chemical vapor deposition processes to predict the observed enhanced growth rates and the deposit properties. Scaling laws are derived that suggest the use of small particle size and high reactant concentration to facilitate complete deposit densification. It is hoped that the model results presented here will guide the development of PECVD processes into parameter ranges producing high-quality material at high deposition rates.

Acknowledgment

This work was supported by the Support of the Department of Energy Office of Conservation Advanced Industrial Materials Program.

Notation

A = total surface area of deposit (internal plus external), cm^2
A_o = area of the bare substrate, cm^2
a_v = local surface area per unit volume, cm^2/cm^3
a_v' = dimensionless local surface area per unit volume
B = empirical constant used in the description of gravitational settling, cm^{-1}
C = concentration of gas phase reacting species, mol/cm^3
C' = concentration of gas phase reacting species, dimensionless
C_o = bulk concentration of gas phase reacting species, mol/cm^3
D = molecular or Knudsen diffusion coefficient, cm^2/s
D_{eff} = effective diffusion coefficient in a porous medium, cm^2/s
Fdr = flow rate of stream of particles having radii in $[r, r+dr]$, cm$^{-2}\cdot$s^{-1}
F_o = flow rate of depositing particle approaching the deposit, cm$^{-2}\cdot$s^{-1}
G = surface growth rate by vapor deposition, cm/s

$g(z)$ = local surface growth rate by vapor deposition, cm/s
$g'(z)$ = dimensionless local surface growth rate by vapor deposition
H = deposit height (thickness), cm
H' = dimensionless deposit height (thickness)
k_s = intrinsic surface rate constant for vapor deposition, $(cm/s)(mol/cm^3)^{-n}$
n = reaction order
$P_s(Z_e)$ = probability that a single given sphere intersects a random volume element at Z_e
P = probability that at least one sphere intersects a random volume element at Z_e
$P_t(Z_p)$ = probability that a depositing sphere reaches Z_p before encountering a solid surface
P_l, P_h = intermediate probabilities in the computation of P_t
R_p = seed particle radius, cm
t = time, s
v_m = molar volume of solid matrix, cm^3/mol
V_s = solid volume fraction
V_{so} = solid volume fraction of bed of packed spheres (no vapor deposition)
V_t = total solid volume deposited per unit substrate area, cm^3/cm^2
z, Z_e, Z_p = distance from substrate surface, cm

Greek letters

α = dimensionless empirical constant (AR_p)
γdr = local number density of spheres with radii in $[r, r+dr]$, $cm^{-3} \cdot cm^{-1}$
ϕ = Thiele modulus
θ = porosity ($1 - V_s$)
η = effectiveness factor
ρ = dimensionless particle radius or radial position (r/Rp)
τ = dimensionless time (tG/R_p)
τ_f = tortuosity factor
Ψ = dimensionless sphere center number density γR_p^4
ζ = dimensionless axial position (z/R_p)
Ω = dimensionless solid volume (V_t/R_p)

Literature Cited

Alam, M. K., and R. C. Flagan, "Controlled Nucleation Aerosol Reactors: Production of Bulk Silicon," *Aerosol Sci. Technol.*, **5**, 237 (1986).

Allen, K. D., and H. H. Sawin, "Thermodynamics of the Silicon-Chlorine-Hydrogen System: Chemical Potential for Homogeneous Nucleation," *J. Electrochem. Soc.*, **133**, 421 (1986).

Baxter, L. L., K. R. Henken, and N. S. Harding, "The Dynamic Variation of Particle Capture Efficiency During Ash Deposition in Coal-Fired Combustors," *Int. Symp. on Comb.*, Orleans, France (1990).

Beddow, J. K., *Particulate Science and Technology*, p. 607, Chemical Publishing Co., New York (1980).

Benenati, R. F., and C. B. Brosilow, "Void Fraction Distribution in Beds of Spheres," *AIChE J.*, **8**, 359 (1962).

Besmann, T. M., R. A. Lowden, B. W. Sheldon, and D. P. Stinton, "Chemical Vapor Infiltration," *Proc. Int. Conf. on Chemical Vapor Deposition*, 482 (1990).

Biswas, P., D. Zhou, I. Zitkovsky, C. Blue, and P. Boolchand, "Superconducting Powders Generated by an Aerosol Process," *Mat. Lett.*, **8**, 233 (1989).

Cannon, W. R., S. C. Danforth, J. H. Flint, J. S. Haggerty, and R. A. Marra, "Sinterable Ceramic Powders from Laser-Driven Reactions: I. Process Description and Modeling," *J. Amer. Ceram. Soc.*, **65**, 324 (1982).

Dullien, F. A. L., "Structural Properties of Packings of Particles," *Handbook of Powder Science and Technology*, p. 112, Van Nostrand Reinhold Co., New York (1984).

Elam, W. T., A. R. Kerstein, and J. J. Rehr, "Critical Properties of the Void Percolation Problem for Spheres," *Phys. Rev. Lett.*, **52**(17), 1516 (1984).

Friedlander, S. K., *Smoke, Dust and Haze: Fundamentals of Aerosol Behavior*, Chap. 3, Wiley, New York (1977).

Gavalas, G. R., "A Random Capillary Model with Application to Char Gasification at Chemically Controlled Rates," *AIChE J.*, **26**(4), 577 (1980).

Henderson, D., M. H. Brodsky, and P. Chaudharl, "Simulation of Structural Anisotropy and Void Formation in Amorphous Thin Films," *Appl. Phys. Lett.*, **25**(11), 641 (1974).

Ho, P., R. J. Buss, and R. E. Loehman, "Glow-Discharge Synthesis of Silicon Nitride Precursor Powders," *J. Mat. Res.*, **4**, 873 (1989).

Leva, M., *Fluidization*, p. 54, McGraw-Hill, New York (1959).

Komiyama, H., and T. Osawa, "Rapid Growth of AIN Films by Particle-Precipitation Aided Chemical Vapor Deposition," *Jap. J. Appl. Phys.*, **24**, L795 (1985).

Komiyama, H., T. Osawa, H. Kazi, and T. Konno, "Rapid Growth of AIN Films by Particle-Precipitation Aided Chemical Vapor Deposition," *Mat. Sci. Monographs*, **38A**, 667 (1986).

Komiyama, H., T. Osawa, Y. Shimogaki, N. Wakita, and T. Ueoka, "Particle Precipitation Aided Chemical Vapor Deposition for Rapid Growth of Ceramic Films: Preparation of 1-mm-Thick AIN, TiO_2 and ZrO_2 Films," *Chem. Vapor Deposition*, p. 1119 (1987).

Krug, J., and P. Meakin, "Microstructure and Surface Scaling in Ballistic Deposition at Oblique Incidence," *Phys. Rev. A*, **40**(4), 2064 (1989).

Meakin, P., "Diffusion-Controlled Deposition on Fibers and Surfaces," *Phys. Rev. A*, **27**(5), 2616 (1983).

Meakin, P., "Ballistic Deposition onto Inclined Surfaces," *Phys. Rev. A*, **38**(2), 994 (1988).

Okoabe, Y., J. Hojo, and A. Kato, "Formation of Fine Silicon Carbide Powders by a Vapor Phase Method," *J. Less-Common Metals*, **68**, 29 (1979).

Racz, Z., and T. Vicsek, "Diffusion-Controlled Deposition: Cluster Statistics and Scaling," *Phys. Rev. Lett.*, **51**(26), 2382 (1983).

Roblee, L. H. S., R. M. Baird, and J. W. Tierney, "Radial Porosity Variations in Packed Beds," *AIChE J.*, **4**, 460 (1958).

Roller, P. S., "The Bulking Properties of Microscopic Particles," *Ind. Eng. Chem.*, **22**, 1206 (1930).

Satterfield, C. N., *Mass Transfer in Heterogeneous Catalysis*, Robert Krieger Publishing Co., Huntington, NY (1981).

Scoville, A. N., and P. Reagan, "Processing and Characterization of Silicon Carbide Components Fabricated via Chemical Vapor Composite Deposition," *Conf. on Composite Materials and Structure*, Cocoa Beach, FL (Jan., 1990).

Shimogaki, Y., and H. Komiyama, "Preparation of Amorphous TiO_2 Films by Thermophoresis-Aided Chemical Vapor Deposition," *Chem. Lett.*, 267 (1986).

Shinohara, K., "Fundamental Properties of Powders: 1. Rheological Properties of Particulate Solids," *Handbook of Powder Science and Technology*, Van Nostrand Reinhold Co., New York (1984).

Spear, K. E., and G. W. Cullen, eds., *Proc. Int. Conf. Chem. Vapor Deposition*, Electrochemical Soc., Pennington (1990).

Stinton, D. P., T. M. Besmann, and R. A. Lowden, "Advanced Ceramics by Chemical Vapor Deposition Techniques," *Amer. Ceram. Soc. Bull.*, **67**, 350 (1988).

Suyama, Y., R. M. Marra, J. S. Haggerty, and H. K. Bowen, "Synthesis of Ultrafine SiC Powders by Laser-Driven Gas Phase Reactions," *Am. Ceram. Soc. Bull.*, **64**, 1356 (1985).

Ulrich, G. D., "Flame Synthesis of Fine Particles," *Chem. Eng. News* (Aug. 6, 1984).

Vold, M. J., "Sediment Volume and Structure in Dispersions of Anisometric Particles," *J. Phys. Chem.*, **63**, 1608 (1960).

Manuscript received May 8, 1991, and revision received Aug. 12, 1991.